Available online at www.sciencedirect.com
ScienceDirect
Acta Materialia 58 (2010) 5063–5069
Acta MATERIALIA
www.elsevier.com/locate/actamat

Comparing calculated and measured grain boundary energies in nickel

Gregory S. Rohrer [a], Elizabeth A. Holm [b,*], Anthony D. Rollett [a], Stephen M. Foiles [b], Jia Li [a], David L. Olmsted [c]

[a] Department of Materials Science and Engineering, Carnegie Mellon University, Pittsburgh, PA 15213-3890, USA
[b] Computational Materials Science and Engineering Department, Sandia National Laboratories, Albuquerque, NM 87185-1411, USA
[c] Department of Materials Science and Engineering, University of California, Berkeley, CA 94720, USA

Received 12 March 2010; received in revised form 19 May 2010; accepted 20 May 2010
Available online 16 June 2010

Abstract

Recent experimental and computational studies have produced two large grain boundary energy data sets for Ni. Using these results, we perform the first large-scale comparison between measured and computed grain boundary energies. While the overall correlation between experimental and computed energies is minimal, there is excellent agreement for the data in which we have the most confidence, particularly the experimentally prevalent Σ3 and Σ9 boundary types. Other CSL boundaries are infrequently observed in the experimental system and show little correlation with computed boundary energies. Because they do not depend on observation frequency, computed grain boundary energies are more reliable than the experimental energies for low population boundary types. Conversely, experiments can characterize high population boundaries that are not included in the computational study. Together the experimental and computational data provide a comprehensive catalog of grain boundary energies in Ni that can be used with confidence by microstructural scientists.
© 2010 Acta Materialia Inc. Published by Elsevier Ltd. All rights reserved.

Keywords: Grain boundary energy; Grain boundary junctions; MD-simulations; EBSD; Serial sectioning

1. Introduction

Grain boundary free energy provides the driving force for grain growth in polycrystalline materials, and as Cyril Smith recognized over 60 years ago, variations in grain boundary energy alter the kinetics and morphology of microstructural evolution [1]. Because of its importance, many investigators have attempted to survey grain boundary energies using various experimental techniques [2–16], but their data sets were limited due to the difficulty of measuring accurate interfacial energies in a bulk solid. Computational models have also been applied, c.f. reviews in Refs. [17–21], but computational restrictions limit data sets primarily to high symmetry boundaries.

Two recent studies have changed this situation. Researchers at Carnegie Mellon University (CMU) [22] and Sandia National Laboratories (SNL) [23] have utilized new, high-throughput methods to measure energy for large ensembles of grain boundaries. Taken together, these studies increase our database of grain boundary energy measurements by orders of magnitude.

The CMU and SNL studies differ in approach – experimental versus computational – and also in sources of uncertainty and error. In this paper, we will compare the CMU and SNL data sets for grain boundary energy in Ni. Our goal is to perform the first large-scale comparison between measured and computed grain boundary energies, in order to develop a comprehensive, validated, well-characterized database of grain boundary energies in Ni that can be used with confidence by microstructural scientists.

2. Method

2.1. Experimental grain boundary energy measurements

2.1.1. Methodology

An experimental method for measuring a large number of relative grain boundary energies in a polycrystalline

* Corresponding author. Tel.: +1 505 844 7669; fax: +1 505 844 9781.
E-mail address: Eaholm@sandia.gov (E.A. Holm).

1359-6454/$36.00 © 2010 Acta Materialia Inc. Published by Elsevier Ltd. All rights reserved.
doi:10.1016/j.actamat.2010.05.042

microstructure has previously been described in detail [24] and applied to MgO [25] and Ni [22] polycrystals. This method presumes that all grain triple junctions are in equilibrium so that each satisfies the Herring condition [26] (i.e. balance of surface tensions and torques). If that is the case, then each triple junction may be characterized by an equation with four (vector) unknowns: three capillarity vectors and the triple junction line vector [27,28]. Since the triple junction line vector may be measured directly, we are left with N equations (one for each triple junction) and $3N$ unknowns (one for each grain boundary).

In order to solve this system of linear equations, we must decrease the number of unknowns. To do this, we make the assumption, first articulated by Brandon [29], that grain boundaries that are close in crystallographic space are similar in energy. Thus, we can group boundaries in energetic bins. Presuming all boundaries in a given bin have the same energy, we reduce the $3N$ unknowns sufficiently to permit solution of the system of equations using an iterative optimization procedure [24]. The result is a set of capillary vectors that can be transformed into grain boundary energies if the grain boundary tangent and normal vectors are known. Because boundary energy is derived from triple junction geometry, the measurement yields boundary energies that are relative to one another, not absolute magnitudes.

Applying this method requires characterizing a large number of equilibrated triple junctions in three spatial dimensions and five crystallographic dimensions. While this would have been prohibitively difficult even a decade ago, new automated techniques now make it tractable. Four of the five macroscopic variables of grain boundary crystallography can be measured efficiently using EBSD and the fifth boundary orientation parameter, which also gives the triple junction geometry, can be observed using serial sectioning and reconstruction techniques. The synthesis of these two methods has yielded large data sets of fully characterized grain boundary ensembles that were analyzed to give the grain boundary character distribution (GBCD) and relative grain boundary energy distribution (GBED) in MgO [25,30] and Ni [22].

2.1.2. Sources of error and uncertainty

To compare these data with other studies, it is important to be aware of sources of non-systematic error (uncertainty) and systematic error (bias). If triple junctions are not in equilibrium, then the Herring condition will not be fulfilled, and calculated energies will be inaccurate for all boundary types. We ensure equilibrium by a careful anneal schedule. Non-systematic errors also arise during the grain boundary reconstruction process, as well described in Ref. [30]; again, these errors should not vary with boundary type but should provide uniform error bars.

The requirement that grain boundaries be binned into groups provides a source of systematic error. Because low-energy cusps are very localized in crystallographic space, low-energy boundaries are inevitably binned with nearby, higher energy boundaries; thus, the experimental measurement method cannot resolve cusps and overestimates the energies of low-energy boundaries. Adjusting the bin width alters, but cannot eliminate, this error because a finite bin width is necessary for the energy calculation to converge.

Finally, the energy measurements are not uniformly distributed among each grain boundary bin. For example, in the Ni specimen a single boundary type, the coherent twin, makes up almost 30% of the boundaries observed, and the $\Sigma 9$ tilt boundary type contributes almost 10%. On the other hand, about 15% of the boundary bins contain fewer than five energy measurements. This nonuniform sampling has two effects. First, calculated energies will be less accurate for less prevalent boundary types simply due to poorer statistics. Second, in the optimization algorithm used to calculate energy, there will be a preference to optimize variables that occur often and thus affect many of the N equations at the expense of variables that affect few equations. The result is that the error increases (perhaps more than predicted by statistical analysis) as the observation frequency decreases.

While these errors are difficult to quantify individually or collectively, it is certainly reasonable to expect error bars on the order of 10%, with larger error bars for less frequently observed boundaries.

2.2. Computational method

2.2.1. Methodology

The computational method for constructing a large catalog of grain boundaries and measuring their energy has been described in detail elsewhere [23]. To avoid bias towards particular boundary types, the method examines all planar boundaries that can be constructed within a periodic cell of a specified maximum size. Having determined which pairs of grain orientations can fit inside the simulation cell, we construct a multiplicity of boundary structures for each orientation pair. We first translate one crystal relative to the other by several offset vectors. For each of the resulting structures, we place the boundary plane at each non-equivalent position. For each of these structures, we remove any overlapping atoms using several different criteria. Finally, we use molecular statics to minimize the $T = 0$ K free energy (i.e. the enthalpy) of each distinct structure. For typical boundaries we minimize several hundred to several thousand configurations; the lowest energy structure is presumed the equilibrium structure.

The material model for these calculations is an embedded atom method (EAM) empirical interatomic potential function [31], parameterized to represent Ni [32]. This particular potential function predicts the stable and unstable stacking fault energies quite accurately, which suggests that it is reasonable to use to examine planar defects such as grain boundaries.

2.2.2. Sources of error

Errors in calculated energies can arise from the boundary construction or minimization processes. While the boundary construction algorithm produces a large number of candidate structures for each grain orientation pair, there is no guarantee that the global minimum energy structure is among them. However, most boundaries evince a large number of nearly degenerate, nearly minimum energy configurations without evidence of low-energy outliers. This suggests that most minimum energy structures are at least reasonable approximations to the true minimum.

Because the boundaries are constructed in a relatively small periodic box, high symmetry boundaries (which often have low energy) are over-represented in the sampling; while this does not induce error in the energy calculations themselves, it does bias the grain boundary distributions toward high symmetry boundaries.

The molecular statics energy minimization calculates the excess enthalpy, rather than the free energy, of the boundaries. It is known that entropic contributions cause the boundary free energy to decrease with temperature by about a factor of three, from 0 K to near the melting temperature [33–35]. It has been presumed that this decrease is similar for most boundaries, and recent studies support this viewpoint, suggesting that free energy scales with the elastic constants up to about 0.75 of the melting temperature [36]. If most boundaries vary with temperature in a similar manner, then the measured enthalpies can be interpreted as relative (but not absolute) free energy values. However, there is the potential that some boundaries do not scale like their peers, perhaps due to structural transformations. The free energy of such boundaries might be poorly represented by their enthalpies. We have no way to determine which, if any, boundaries are so affected.

Finally, as with all empirical atomistic simulations, errors can arise from the physical model for atomic interactions, i.e. the EAM interatomic potential function. Different potential functions for the same material can give substantially different property values, depending on which parameters were used to fit the function. For calculating grain boundary energies, we select a potential well suited to planar defects. This potential was fit to the stacking fault energy and low-index surface energies and yields values of 127 mJ m^{-2} for the stacking fault energy and low-index surface energies ranging from 1950 to 2375 mJ m^{-2}. These compare well with the experimental values of 125 mJ m^{-2} for the stacking fault and an average surface energy of 2280 mJ m^{-2} [37]. Because the atomic environment differs from a stacking fault or low-index surface more in a high energy grain boundary than in a low-energy boundary, we might expect the error to increase with boundary energy. While the error in the computed grain boundary energies is difficult to quantify in the absence of high fidelity boundary energy data, typical error bars of 10% seem reasonable, with the caveat that the error may not be constant in boundary energy.

2.3. Comparing experimental and computational data

The experimental data set for polycrystalline Ni grain boundaries is described in Ref. [22]; 37,000 triple junctions were analyzed to provide approximately 10^5 grain boundary free energy measurements. The grain boundaries were discretized into equal volume bins that span approximately 8.2° of all five angular parameters such that there are 17,894 discrete grain boundary types. The parameterization and equal volume binning procedure, which account for all symmetries and multiplicities of the crystal system, are described in Ref. [38]. Computational results indicate that the energies of boundaries within about 10° of each other are well correlated [23], so the 8.2° bin size is reasonable. It is worth noting that the experimental data set includes both the distribution of grain boundary types in crystallographic space (i.e. the GBCD) and the extracted energy distribution (i.e. the GBED). The GBCD, which is measured directly, is considered to be more accurate than the GBED, which is a derived quantity.

The computational data set for Ni bicrystal boundaries is described in Refs. [23] and is publicly available as online supplemental material to that paper; 388 distinct grain boundaries were constructed and characterized. To compare these boundaries to the experimental data, we extract the rotation angle and axis and boundary plane for each and apply all possible face-centered cubic (fcc) symmetry operators. For each equivalent boundary, we identify the appropriate grain boundary type (i.e. bin) in the experimental system and read the energy. The average energy for all the equivalent boundaries is taken as the relevant experimental energy, to be compared to the calculated value.

3. Results and discussion

3.1. All boundaries

Fig. 1a compares the experimental and calculated grain boundary energy for all 388 boundaries in the computational data set. Taken in aggregate, the calculated and measured energies show little correlation (unweighted correlation coefficient $R_U = +0.18$) and the linear curve fit is unconvincing. For both sets, the lowest energy boundary is the coherent twin (60°/[1 1 1], pure twist) and, in general, boundaries with higher measured energies have higher calculated energies. However, the distribution is broad and there are a significant number of outliers.

A challenge to interpreting this data arises from the unknown error bars. As discussed above, we expect the uncertainty in the experimental grain boundary energies to increase as the observation frequency decreases. The boundary population per bin, P, varies widely in the experimental data set, from 0.12 to 4500 times the population we would expect in a purely random system (termed multiples of a random distribution, MRD). If we weight the experimental energy measurements by P, we obtain a linear fit

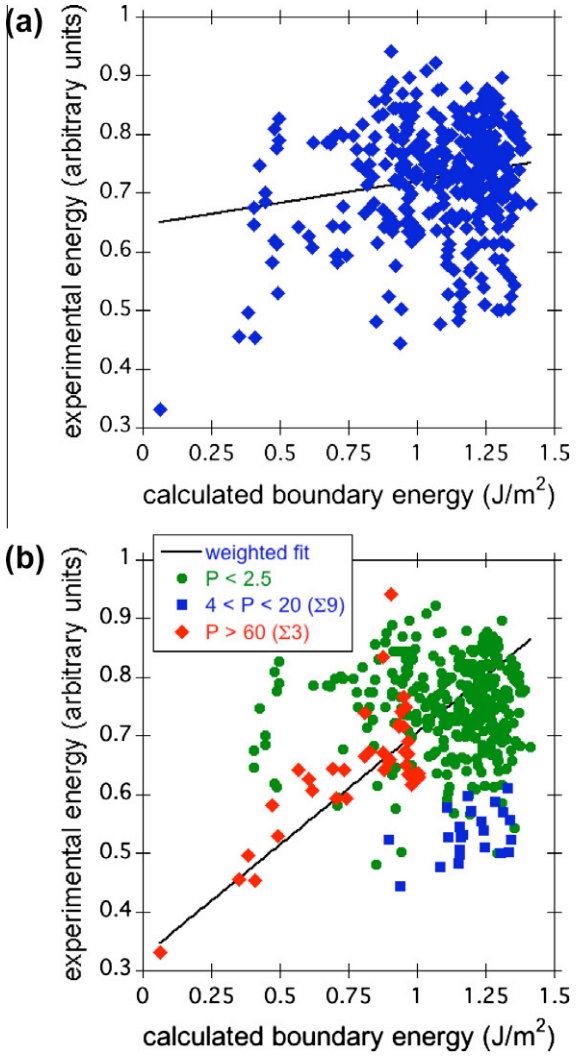

Fig. 1. The relationship between experimental and calculated grain boundary energy in Ni. (a) An unweighted linear fit to all the data (solid line) shows little correlation and is not a good representation of the data. (b) A linear fit weighted by boundary population, P, shows much higher correlation and is a better representation of the data. Note that the data fall into three population groups: $P > 60$ (red diamonds), $4 < P < 20$ (blue squares), and $P < 2$ (green circles).

to the calculated energies with a much higher correlation coefficient (weighted correlation coefficient $R_W = +0.92$), as shown in Fig. 1b. The curve fit is intuitively more pleasing and fits the low-energy boundaries, where we expect the most accurate data, especially well. Thus, the correlation between experimental and calculated grain boundary energy is very strong for the data in which we have the most confidence.

It is interesting to observe that the boundaries form three distinct and separate clusters in population space, as shown in Fig. 1b. The high population bins, with $P > 60$ MRD, each contain 300 or more measurements, and the curve fit is heavily weighted toward these boundary types; this group includes only the Σ3 boundaries. The mid-population bins, with $4 < P < 20$, contain 20 or more measurements per bin and include only Σ9 boundaries. Intriguingly, they seem to suggest a different linear fit between experiment and simulation; the implications will be discussed below. The low population bins, with $P < 2.5$, contain fewer than 16 measurements each, and most of these bins contain fewer than five measurements. We would not expect the data quality to be high for these sparse bins, and indeed, there is substantial scatter about the linear fit.

Because high-energy boundaries are preferentially eliminated during grain growth (c.f. Refs. [39–41]), we expect that low-energy boundary bins will be more populated than high-energy bins in the experimental data. Fig. 1b confirms this trend, although there are outliers.

3.2. Σ3. and Σ9 boundaries

Coherent and incoherent Σ3 boundaries are the most frequently observed in the experimental system, comprising almost 40% of the total grain boundary length. Because of their high symmetry, they are also well represented in the computational data, where 41 of the 388 simulated boundaries are of Σ3 type. Fig. 2a shows experimental and computed energies for Σ3 boundaries; as these were the most strongly weighted data in the overall fit, they unsurprisingly show even stronger correlation when considered separately ($R_U = 0.71$, $R_W = 0.95$). There are two apparent outliers, a (10 2 2)/(1 1 1) and an (8 1 1)/(5 4 4) boundary, circled in Fig. 2a. However, neither boundary corresponds to a local minimum in the relative boundary area distribution, as would be expected for a high-energy boundary. Combined with the fact that they are not consistent with the calculated energies, we consider these data questionable. With the two outliers excluded, the correlation improves slightly ($R_U = 0.80$, $R_W = 0.98$).

In polycrystals with many Σ3 boundaries, there is a tendency for Σ3 boundaries to form Σ3–Σ3–Σ9 triple junctions (c.f. Ref. [42]), which was confirmed in this system [22]. Σ9 boundaries are the second most prevalent boundaries in the experimental data set, and 23 of the 388 simulated boundaries are Σ9 type. However, the computational boundary set included only four of the most experimentally prevalent Σ9 boundaries, the low-energy Σ9 tilt boundaries. Fig. 2b shows the experimental and computed energies for Σ9 boundaries. There is a modest correlation ($R_U = 0.43$, $R_W = 0.48$), which we would expect to improve if additional highly populated Σ9 boundary types observed in experiments were included in the comparison.

In twinned or grain boundary engineered materials, the Σ3 and Σ9 boundaries often form a network of boundaries and triple junctions that is relatively distinct from the high angle boundary network [42]. This implies that the triple junction equilibrium equations, which are minimized to calculate energy, may be divided into two disjoint types: Σ3–Σ3–Σ9 triple junctions and other boundary junctions. The two groups have quite different computational characteristics, and it is possible that the optimization algorithm

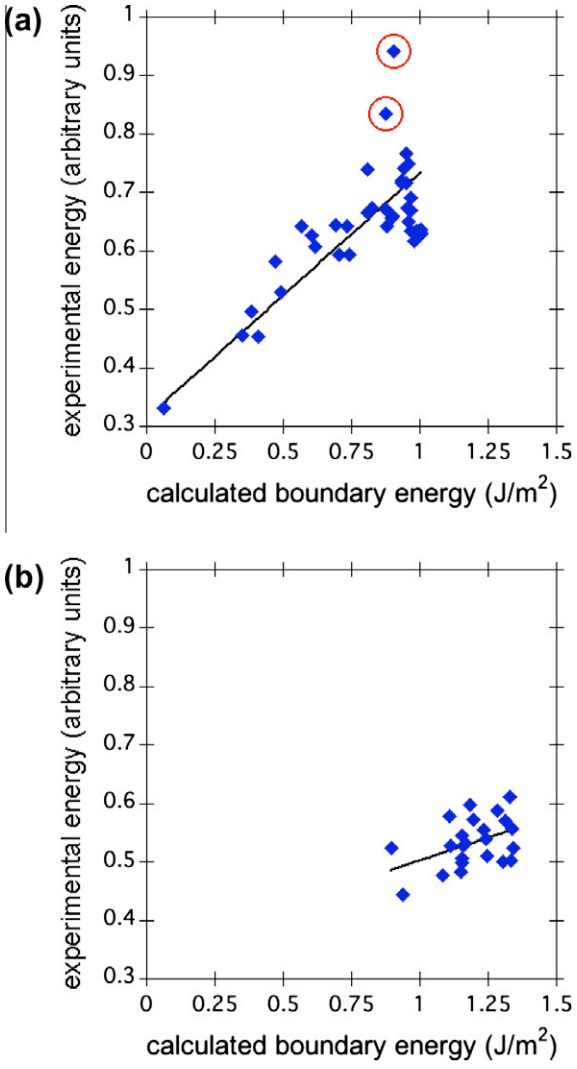

Fig. 2. The relationship between experimental and calculated grain boundary energy for CSL grain boundaries in Ni. (a) Σ3 boundaries show a strong correlation between experimental and calculated energy. The two circled points are outliers in the experimental energy distribution that do no correspond to minima in the experimental population distribution, so are considered questionable. (b) Σ9 boundaries show a weaker correlation between experimental and calculated energy.

optimizes each separately, assigning different relative energies to each set. This possibility requires further study.

3.3. Other boundaries

Other CSL boundary types, including Σ5, Σ7, Σ11 and Σ15, are well represented among the simulated boundaries. However, few of the simulated CSL boundaries are observed in the experimental data set at even the random frequency (i.e. $P < 1$ MRD for nearly all boundary types). As expected for low population boundaries, we see at best modest correlation between the experimental and computational energies for these boundaries. Furthermore, the slopes of the linear fits vary widely with boundary type, indicating that the correlation between data sets does not arise from proportionality between experimental and calculated energy.

It is interesting to consider how many additional experimental measurements would be required to resolve the energies of infrequently observed boundaries. Observation frequencies of high population boundaries are about two orders of magnitude higher than low population boundaries. Thus, to achieve confidence in low population boundary energies comparable to that of high population boundary energies would require about 10^2 times more measurements than in the current data set. In this Ni system, that implies about 4×10^6 triple junction characterizations, which is currently an intractable size. In other materials, different boundary populations may require different system sizes. For example, because Al polycrystals lack the Σ3 and Σ9 boundary subnetwork seen in Ni, the boundary population distribution may be more uniform in Al, permitting smaller experimental system sizes.

Because the computed energies are not dependent on an observation frequency, their validity should not vary with population. (Although since many low population boundaries are of high energy, systematic errors in energy might be operative, as discussed above.) Furthermore, the good correlation between experimental and computed energies for high population boundaries at all observed energies suggests that the computed energies are physically realistic and representative. Thus, our conclusion is that the computed grain boundary energies may be more reliable than the experimental energies for low population boundary types and can be used to approximate energies of boundaries that are experimentally inaccessible.

On the other hand, the experimental studies indicate that certain commonly simulated boundaries are not present in significant numbers in real microstructures and cannot be considered typical boundaries. For example, a number of computational studies have used the Σ5 symmetric tilt boundary as a model high angle boundary (c.f. Refs. [43–45]). The GBCD data for Ni indicate that this boundary is rarely observed, with a population $P < 0.4$ MRD. Likewise, some frequently observed boundaries, such as most of the Σ9 tilt boundaries, were not included in the computational boundary catalog. Clearly, experiments can guide computational boundary selection to ensure that relevant and important boundary types are examined.

3.4. Boundary population correlations

While the grain boundary energy distribution is extracted from the grain boundary character distribution along with other geometric measurements, the GBCD is measured directly and has fewer sources for error. Both experimental [22,25] and computational [39,40] studies have indicated that the population of grain boundaries in a polycrystal is inversely proportional to their energies, or the GBCD scales with the reciprocal of the GBED. Because the GBCD is a potentially more reliable experi-

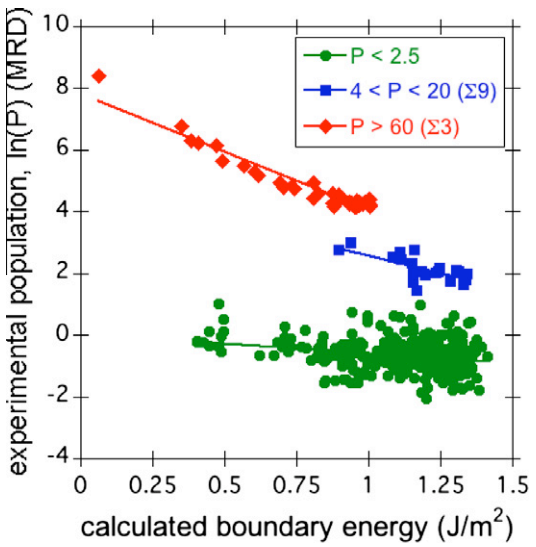

Fig. 3. The relationship between experimental GBCD and calculated GBED in Ni. For high population Σ3 and mid-population Σ9 boundaries, the inverse correlation between GBCD and GBED (solid lines) is stronger than the direct correlation between experimental and calculated GBEDs. However, the low population boundaries remain poorly correlated, due to high experimental uncertainty.

mental measure, it is possible that the computed GBED correlates more strongly with the experimental GBCD than with the experimental GBED.

Fig. 3 compares the experimental GBCD with the computational GBED. Note that because boundary populations vary over a wide range, the GBCD is plotted as $\ln(P)$. The three population groups described above are indicated in the figure; they are clearly distinct groups. Although a linear fit to the complete data set shows modest correlation ($R_U = 0.45$), the actual line is placed between the high P and low P boundary clusters and bears little resemblance to the data set. However, the linear fit to the high P Σ3 boundary data gives a good fit and a much higher unweighted correlation coefficient ($R_U = 0.96$) than observed in the GBED comparison. (Note that in these fits, we do not weight by population, since population is the dependent variable.) In addition, the outliers that were present in the GBED data are absent here, again indicating that those energy measurements are spurious. The Σ9 fit is also improved relative to the GBED comparison, with $R_U = 0.69$. For low P boundaries, the GBCD data correlate with computed energy more strongly than the experimental GBED do, but the correlation is still poor ($R_U = 0.24$), re-emphasizing the dependence of data quality on observation frequency.

Overall, the experimental GBCD data provide a better correlation to the computed GBED. Since the GBCD is more straightforward to characterize experimentally than the GBED, it offers a more accessible metric for comparison to computed boundary energies. However, the improved correlation cannot compensate for the lack of observation data in low P boundary bins. For those boundaries, the computed energy remains more reliable than the experimental data.

4. Conclusions

Recent independent experimental and computational studies have produced two large sets of grain boundary energy data for Ni [22,23]. The data were obtained by different approaches with distinct sources of error and uncertainty. The experimental data set contains a large number of relative grain boundary free energies binned into 17,894 boundary types. The computational data set includes only 388 boundaries, and the enthalpy of each boundary is characterized individually. Our comparisons between the experimental and computed boundary energies suggest several conclusions:

1. The unweighted correlation between experimental and computed grain boundary energies is minimal.
2. There is a strong correlation between the experimental and calculated energies when the fit is weighted by the experimental observation frequency. Because the quality of the experimental data scales with the observation frequency, we conclude that there is excellent agreement between experiment and computation for the data in which we have the most confidence.
3. For Σ3 boundary types, which are the most frequently observed boundaries in the experimental polycrystal, the correlation between experiment and computation is even stronger.
4. The next most populous boundaries, the Σ9 boundaries, show a modest correlation between experiment and computation. Other CSL boundaries are infrequently observed in the experimental system and show little correlation with computed boundary energies.
5. Boundary population can be used to determine the experimental system size required to achieve a desired accuracy in energy measurements. Different materials systems will require different system sizes.
6. Because they do not depend on observation frequency, computed grain boundary energies may be more reliable than the experimental energies for low population boundary types and can be used to approximate the energies of boundaries that are experimentally inaccessible.
7. The computational data set excludes some frequently observed boundaries and includes some infrequently observed boundaries. Experiments should guide future computational studies to ensure that relevant and important boundary types are examined.
8. The grain boundary character distribution, which can be measured more easily than the energy distribution, offers a strong inverse correlation to computed grain boundary energies and can be used in place of the grain boundary energy distribution in comparisons with computed energies.

Overall, the experimental and computational results validate each other for boundaries that are appropriately represented in both data sets. By understanding the limitations of each method, we can combine experimental and computational data to achieve a more comprehensive catalog of grain boundary energies in Ni that can be used with confidence by microstructural scientists.

Acknowledgements

Sandia is a multi-program laboratory operated by Sandia Corporation, a Lockheed Martin Company, for the US Department of Energy's National Nuclear Security Administration under contract DE-AC0494AL85000. We acknowledge support from the Department of Energy, Office of Basic Energy Sciences both through the core program and through the Computational Materials Science Network program. The work at CMU was primarily supported by the MRSEC program of the National Science Foundation under Award Number DMR-0520425.

References

[1] Smith CS. Grain shapes and other metallurgical applications of topology. In: Metal interfaces. Cleveland (OH): ASM; 1952. p. 65–108.
[2] Read WT, Shockley W. Phys Rev 1950;78:275–89.
[3] Hasson G, Boos J-Y, Herbeuval I, Biscondi M, Goux C. Surf Sci 1972;31:115–37.
[4] Barmak K, Kim J, Kim K-S, Archibald WE, Rohrer GS, Rollett AD, et al. Scripta Mater 2006;54:1059–63.
[5] Gjostein NA, Rhines FN. Acta Metall 1959;7:319–30.
[6] Hasson GC, Goux C. Scripta Metall 1971;5:889–94.
[7] McLean M. J Mater Sci 1973;8:571–6.
[8] Chan SW, Balluffi RW. Acta Metall 1985;33:1113–9.
[9] Chan SW, Balluffi RW. Acta Metall 1986;34:2191–9.
[10] Schmelzle R, Muschik T, Gust W, Predel B. Scripta Metall Mater 1991;25:1981–6.
[11] Wolf U, Ernst F, Muschik T, Finnis MW, Fischmeister HF. Philos Mag A – Phys Condens Matter Struct Defects Mech Prop 1992;66:991–1016.
[12] Miura H, Kato M, Mori T. J Mater Sci Lett 1994;13:46–8.
[13] Straumal BB, Polyakov SA, Bischoff E, Gust W, Mittemeijer EJ. Interf Sci 2001;9:287–92.
[14] Skidmore T, Buchheit RG, Juhas MC. Scripta Mater 2004;50:873–7.
[15] Amouyal Y, Rabkin E, Mishin Y. Acta Mater 2005;53:3795–805.
[16] Amouyal Y, Rabkin E. Acta Mater 2007;55:6681–9.
[17] Sutton AP. Int Met Rev 1984;29:377–402.
[18] Sutton AP, Balluffi RW. Acta Metall 1987;35:2177–201.
[19] Sutton AP, Vitek V. Philos Trans Roy Soc Lond Ser A, Math Phys Sci 1983;309:55–68.
[20] Wang G-J, Vitek V. Acta Metall 1986;34:951–60.
[21] Wolf D, Merkle KL. Correlation between the structure and energy of grain boundaries in metals. In: Wolf D, Yip S, editors. Materials interfaces: atomic-level structure and properties. London: Chapman-Hall; 1992. p. 87–150.
[22] Li J, Dillon SJ, Rohrer GS. Acta Mater 2009;57:4304–11.
[23] Olmsted D, Foiles SM, Holm EA. Acta Mater 2009;57:3694–703.
[24] Morawiec A. Acta Mater 2000;48:3525–32.
[25] Saylor DM, Morawiec A, Rohrer GS. Acta Mater 2003;51:3675–86.
[26] Herring C. The use of classical macroscopic concepts in surface energy problems. In: Gomer R, Smith CS, editors. Structure and properties of solid surfaces. Chicago: The University of Chicago Press; 1952. p. 5–81.
[27] Cahn JW, Hoffman DW. Acta Metall 1974;22:1205–14.
[28] Hoffman DW, Cahn JW. Surf Sci 1972;31:368.
[29] Brandon DG. Acta Metall 1966;14:1479–84.
[30] Saylor DM, Morawiec A, Rohrer GS. Acta Mater 2003;51:3663–74.
[31] Daw MS, Foiles S, Baskes MI. Mater Sci Rep 1993;9:251–310.
[32] Foiles SM, Hoyt JJ. Acta Mater 2006;54:3351–7.
[33] Foiles SM. Phys Rev B 1994;49:14930–8.
[34] Broughton JQ, Gilmer GH. J Phys Chem 1987;91:6347–59.
[35] Broughton JQ, Gilmer GH. Modell Simulat Mater Sci Eng 1998;6:393–404.
[36] Foiles SM. Scripta Mater 2010;62:231–4.
[37] Hirth JP, Lothe J. Theory of dislocations. 2nd ed. New York: John Wiley & Sons; 1982.
[38] Rohrer GS, Saylor DM, Dasher BE, Adams BL, Rollett AD, Wynblatt P. Z Matallkunde 2004;95:197–214.
[39] Holm EA, Hassold GN, Miodownik MA. Acta Mater 2001;49:2981–91.
[40] Upmanyu M, Hassold GN, Kazaryan A, Holm EA, Wang Y, Patton B, et al. Interf Sci 2002;10:201–16.
[41] Dillon SJ, Rohrer GS. Acta Mater 2009;57:1–7.
[42] Randle V. Mater Sci Technol 2010;26:253–61.
[43] Sorensen MR, Mishin Y, Voter AF. Phys Rev B 2000;62:3658–73.
[44] Campbell GH, Plitzko JM, King WE, Foiles SM, Kisielowski C, Duscher GJM. Interf Sci 2004;12:165–74.
[45] Zhang H, Srolovitz DJ. Acta Mater 2006;54:623–33.